

# A Comparative Study of UMAP and Other Dimensionality Reduction Methods \*

Guanzhe Zhang<sup>†</sup>, Shanshan Ding<sup>†</sup>, and Zhezhen Jin<sup>‡</sup>

<sup>†</sup>Department of Applied Economics and Statistics, University of Delaware

<sup>‡</sup>Department of Biostatistics, Columbia University

## Abstract

Uniform Manifold Approximation and Projection (UMAP) is a widely used manifold learning technique for dimensionality reduction. This paper studies UMAP, supervised UMAP, and several competing dimensionality reduction methods, including Principal Component Analysis (PCA), Kernel PCA, Sliced Inverse Regression (SIR), Kernel SIR, and t-distributed Stochastic Neighbor Embedding, through a comprehensive comparative analysis. Although UMAP has attracted substantial attention for preserving local and global structures, its supervised extensions, particularly for regression settings, remain rather underexplored. We provide a systematic evaluation of supervised UMAP for both regression and classification using simulated and real datasets, with performance assessed via predictive accuracy on low-dimensional embeddings. Our results show that supervised UMAP performs well for classification but exhibits limitations in effectively incorporating response information for regression, highlighting an important direction for future development.

**Key Words:** dimension reduction; supervised dimension reduction; linear embedding; nonlinear embedding; regression; classification

---

\*The authors gratefully acknowledge the support from NSF DMS-2413833, NIH DE-CTR ACCEL U54-GM104941, and NIH NIGMS DE-INBRE P20 GM103446 for Ding’s research, and NSF DMS-2413834, NIH U19 AG068054 ABC-DS, and NIH U19 AG063893 LLF Study for Jin’s research.

# 1 Introduction

Dimensionality reduction is crucial in data science and machine learning, especially when working with high-dimensional datasets. It simplifies data for visualization, classification, and other tasks while preserving important structures and reducing complexity [1]. Recent efforts have focused on improving the scalability, clarity, and capacity to manage intricate, non-linear relationships in data. Techniques such as deep learning autoencoders, manifold learning methods, and kernel-based approaches have expanded the range for dimensionality reduction methods, promoting more robust analysis of complex and high-dimensional datasets, particularly in the fields of genomics, image processing, and natural language processing [2, 3, 4]. These methods address challenges where high-dimensional data can lead to overfitting and computational inefficiency [5, 6, 7, 8].

In this paper, we study Uniform Manifold Approximation and Projection (UMAP) in both unsupervised and supervised settings, together with several competing dimensionality reduction methods, including PCA, Kernel PCA (KPCA), t-distributed Stochastic Neighbor Embedding (t-SNE), SIR, and kernel SIR (KSIR). While existing studies of supervised UMAP have focused primarily on classification problems, its behavior and effectiveness in regression settings remain largely unexplored. We conduct a systematic empirical evaluation of supervised UMAP for regression and classification, assessing its ability to retain predictive information in the reduced representation and comparing its performance with alternative dimension reduction approaches. Our results demonstrate the strengths and limitations of supervised UMAP for supervised learning tasks and provide guidance for its practical applications.

UMAP, developed by McInnes, Healy, and Melville (2018), is a manifold learning method designed to preserve both local and global structure when reducing high dimensional data to low dimensional representations [9]. Based on robust topological foundations, it utilizes concepts such as fuzzy simplicial sets and Riemannian geometry to form low-dimensional representations of the original data. Compared with other non-linear dimensionality reduction

methods, such as t-SNE, UMAP often provides improved preservation of global structures while maintaining computational efficiency [4]. Subsequent developments have expanded its applicability, including Parametric UMAP, which leverages neural networks to enable scalable embeddings and efficient out-of-sample extension [10]. Supervised UMAP, proposed as an extension of the original UMAP framework, incorporates response information into the embedding process to preserve relationships between predictors and outcomes in the reduced low dimensional space [9]. It accommodates both categorical and continuous responses and has been applied in a wide range of supervised learning contexts, particularly in classification settings, including but not limited to genomics, natural language processing, neuroscience, and image analysis [9, 4, 11, 12, 13, 14, 15].

Among other competing dimensionality reduction methods, PCA is one of the most well-known linear dimensionality reduction methods [16, 17]. It identifies orthogonal linear combinations of features that maximize variance, thereby preserving information in terms of variability. The primary advantages of PCA are its simplicity and interpretability [18, 19]. However, it assumes that variance is the most important structure in the data, and is sensitive to scaling and limited in capturing nonlinear feature relationships [19, 20]. This limitation motivated Kernel PCA, which captures nonlinear structure through kernel mappings [21, 22]. PCA and its nonlinear extensions do not incorporate response information when performing dimensionality reduction, which can limit their utility in supervised learning tasks [1].

SIR, introduced by Li (1991), is a supervised dimensionality reduction method designed for both regression and classification problems. SIR seeks low-dimensional linear combinations of predictors that capture the essential relationship between the predictors and the response [23, 24, 25, 26]. Unlike PCA, which ignores response information, SIR explicitly incorporates the response to identify informative directions for supervised learning. The method assumes that the response depends on a small number of linear combinations of the predictors and operates by partitioning the response into slices and estimating conditional means of the predictors within each slice to recover the central subspace. SIR relies on a linearity

condition. This assumption has been shown to be relatively mild in high-dimensional settings [27, 28, 29], and the method has demonstrated strong empirical performance across a wide range of applications, including genomics, econometrics, financial modeling, and image analysis ([30, 31, 32, 33, 34], among others). As with PCA, SIR may be limited in its ability to capture nonlinear relationships. Kernel SIR addresses this limitation by extending SIR to a reproducing kernel Hilbert space to enable the recovery of nonlinear predictor–response relationships while retaining the supervised structure of the original method.

t-SNE, developed by van der Maaten and Hinton (2008), is a widely used non-linear dimensionality reduction and data visualization technique [35]. It constructs low-dimensional embeddings by minimizing the divergence between probability distributions of pairwise similarities in the high- and low-dimensional spaces, using Gaussian kernels in the original space and a Student’s t-distribution in the embedding to mitigate the crowding problem [36]. t-SNE is particularly effective at preserving local structure and revealing cluster patterns, and has been widely applied to biological data, text embeddings, and image representations [14]. Compared with PCA, t-SNE excels at visualizing nonlinear structure and is well suited for unsupervised exploratory analysis [37]. However, it does not provide an explicit mapping for new data, requiring recomputation of the embedding when additional observations are introduced [38, 39].

Although UMAP has gained significant attention for its ability to preserve both local and global data structures in low-dimensional embeddings, research on its supervised extensions remains rather underdeveloped, particularly in regression settings. Existing work has focused largely on classification or qualitative visualization, leaving an important knowledge gap in understanding the performance of supervised UMAP for continuous outcomes. To address this limitation, we investigate supervised UMAP in both classification and regression settings, with a particular emphasis on its performance in regression frameworks. The proposed study provides a comprehensive empirical evaluation of its performance under different modeling conditions and compares it against several widely used dimension reduction and

sufficient dimension reduction techniques. To our knowledge, this is the first systematic empirical evaluation of supervised UMAP for both regression and classification problems. It also provides the first comparative study between supervised UMAP and popular sufficient dimension reduction methods, such as SIR and kernel SIR. The study shows that while supervised UMAP performs well in classification, it has limitations to effectively incorporate response information for dimension reduction in regression settings, indicating an important need for improved methods and an important direction for future research.

The rest of the paper is organized in the following way: In section 2, we provide a detailed overview of the methodologies of the dimensionality reduction methods; In section 3, we describe the process of generating the simulated data, including their feature distributions and models to create response variables. We further introduce two real-world datasets used in this study and explain how the evaluation process is structured and performed; Section 4 presents comprehensive comparative numerical results and visualizations, along with a detailed analysis of the findings across methods. Section 5 concludes the paper with a summary of key results and directions for future research.

## 2 Methodology

This section provides the technical background of unsupervised UMAP, supervised UMAP, and other dimensionality reduction methods. Let  $X_1, X_2, \dots, X_n \in \mathbb{R}^p$  be  $p$ -dimensional predictors and  $Y_1, Y_2, \dots, Y_n \in \mathbb{R}$  be univariate response variables.

### 2.1 UMAP and Supervised UMAP

UMAP can be developed in both unsupervised and supervised settings. In the unsupervised setting, UMAP utilizes only the feature data to construct embeddings that preserve the global and local structures of the high-dimensional data in a lower-dimensional space [9].

In particular, UMAP builds a fuzzy graph in the following way [9]: For each high-

dimensional data point  $X_i \in \mathbb{R}^p$ , UMAP identifies the  $k$  nearest neighbors and computes distances between  $X_i$  and its neighbors  $X_j$ ,  $1 \leq j \leq k$ , denoted as  $d(X_i, X_j)$  using a distance metric (e.g., Euclidean).

1. For each  $X_i$ , define  $\rho_i$  and  $\sigma_i$ :

$$\rho_i = \min \{d(X_i, X_j) \mid 1 \leq j \leq k, d(X_i, X_j) > 0\}, \quad (1)$$

$$\sum_{j=1}^k \exp \left( -\frac{\max(0, d(X_i, X_j) - \rho_i)}{\sigma_i} \right) = \log_2(k), \quad (2)$$

where  $\rho_i$  is the distance to the closest neighbor and  $\sigma_i$  is a local scaling parameter.

2. Using the two parameters above, construct a similarity graph for data points. For each edge from  $X_i$  to its neighbor  $X_j$ , define the weight function as:

$$w_{ij} = w(X_i, X_j) = \exp \left( -\frac{\max(0, d(X_i, X_j) - \rho_i)}{\sigma_i} \right). \quad (3)$$

Symmetrize the weighted graph by modifying the edge weight as:

$$\tilde{w}_{ij} = w_{ij} + w_{ji} - w_{ij}w_{ji}. \quad (4)$$

Here  $\tilde{w}_{ij}$  can be considered as the probability that the given edge exists.

3. Define the strength of two data points  $z_i, z_j \in \mathbb{R}^d$  in the low-dimensional space as:

$$\Phi(z_i, z_j) = \left( 1 + a (\|z_i - z_j\|_2^2)^b \right)^{-1}, \quad (5)$$

where  $a$  and  $b$  are fixed global parameters and are chosen to approximate a target curve  $g(s)$ :

$$\min_{a,b} \sum_{s \in \mathbb{R}_{\geq 0}} \left[ \frac{1}{1 + a s^{2b}} - g(s) \right]^2$$

with  $s = \|z_i - z_j\|_2$ ,  $g(s) = 1$  if  $s \leq \text{min\_dist}$  and  $g(s) = \exp(-(s - \text{min\_dist}))$  if  $s > \text{min\_dist}$ . Here  $\text{min\_dist}$  is a hyperparameter that defines the minimum distance between embedded points that are connected.

The term  $\Phi(z_i, z_j)$  defined in (5) can be interpreted as the probability that the two points are connected in the corresponding low-dimensional space, which approaches one as their distance is close to zero and decays in a heavy-tailed pattern as their distance increases. UMAP finds the low-dimensional embeddings  $\{z_i \in \mathbb{R}^d\}$  by minimizing a cross-entropy loss  $C$  between  $\tilde{w}_{ij}$  and  $\Phi(z_i, z_j)$  using stochastic gradient descent optimization, where

$$C = - \sum_{i,j} [\tilde{w}_{ij} \log(\Phi(z_i, z_j)) + (1 - \tilde{w}_{ij}) \log(1 - \Phi(z_i, z_j))]. \quad (6)$$

The initial values of the low-dimensional embeddings in the optimization are obtained through spectral embeddings of the weighted nearest-neighbor graph in the original high-dimensional space [9].

In supervised UMAP, response information is incorporated to enhance the embeddings. How to utilize response information depends on whether the response variable is categorical or continuous, which influences how the response information is integrated into the embedding process. Specifically, supervised UMAP incorporates the information from response variables to modify the construction of the high-dimensional graph and uses it for subsequent computations, while keeping the other steps in the process unchanged. For datasets with categorical response variables, supervised UMAP modifies its similarity graph to pull closer those data points that share the same label and push apart those with different labels. It achieves this by adjusting the edge weights to reward connections between data points with

the same label and penalize those with different labels as follows [40, 41]:

$$w_{ij}^{sup} = w_{ij} \times \begin{cases} e^{-f}, & \text{if labels differ,} \\ 1, & \text{if labels match.} \end{cases} \quad (7)$$

Here

$$f = \begin{cases} 2.5 \times \frac{1}{1-\alpha}, & \text{if } \alpha < 1 \\ +\infty, & \text{if } \alpha = 1, \end{cases} \quad (8)$$

where  $\alpha$  is a consistent parameter with a value typically between 0 and 1. After the adjustment, it replaces  $w_{ij}$  with  $w_{ij}^{sup}$  as the edge weight in the similarity graph for the symmetrization and the following process.

For datasets with continuous response variables, the existing supervised UMAP calculates the similarity of numerical response  $Y_i \in \mathbb{R}$  using the same way as it does for computing feature similarity and combines it with feature similarity [40, 41]. After defining a response distance  $d(Y_i, Y_j)$ , the supervised UMAP builds a fuzzy graph for responses in the following way:

$$\rho_{i,y} = \min \{d(Y_i, Y_j) \mid 1 \leq j \leq k, d(Y_i, Y_j) > 0\}, \quad (9)$$

$$\sum_{j=1}^k \exp \left( -\frac{\max \{0, d(Y_i, Y_j) - \rho_{i,y}\}}{\sigma_{i,y}} \right) = \log_2(k). \quad (10)$$

where  $\rho_{i,y}$  is the distance to the closest neighbor in responses and  $\sigma_{i,y}$  is a local scaling parameter. Then compute the response similarity as:

$$w_{ij,y} = \exp \left( -\frac{\max (0, d(Y_i, Y_j) - \rho_{i,y})}{\sigma_{i,y}} \right). \quad (11)$$

Combine it with the edge weight  $w_{ij}$ ,

$$w_{ij}^{sup} = \begin{cases} w_{ij} \cdot (w_{ij,y})^{\frac{1-\alpha}{\alpha}}, & \alpha < 0.5, \\ (w_{ij})^{\frac{\alpha}{1-\alpha}} \cdot w_{ij,y}, & \alpha \geq 0.5. \end{cases} \quad (12)$$

where  $\alpha$  is a tuning parameter with a value typically between 0 and 1, controlling how strongly the responses impact the overall graph [40, 41]. Then, supervised UMAP uses  $w_{ij}^{sup}$  as the edge weight in the similarity graph for the symmetrization and the remaining process.

The existing supervised UMAP method for continuous responses may overfit by directly incorporating distance measures based on the response variable. To mitigate this issue, we propose an alternative way that discretizes the response by slicing it into non-overlapping intervals and treating each interval as a categorical label. Supervised UMAP is then applied using edge weights defined in (7) to construct the embedding. This approach reduces overfitting relative to the existing supervised UMAP method, but it still exhibits limitations for dimensionality reduction in regression settings, as shown in Section 4.

## 2.2 PCA and KPCA

PCA is an unsupervised linear method that reduces dimensionality by projecting the data onto a set of orthogonal components that capture the maximum variance in the dataset [16, 17, 18]. It finds the principal components by performing eigenvalue decomposition for the covariance matrix of the original features. Given a dataset of  $n$  samples  $\{X_1, X_2, \dots, X_n\}$ , with each  $X_i \in \mathbb{R}^p$ , let's denote the data matrix as  $X \in \mathbb{R}^{n \times p}$  and center the data matrix as  $X_C$ . The covariance matrix  $\Sigma$  is computed as  $\Sigma = \frac{1}{n} X_C^T X_C$ . After spectral decomposition on  $\Sigma$ , sort eigenvectors in a descending order of their corresponding eigenvalues, and let  $W \in \mathbb{R}^{p \times k}$  be the matrix whose columns are the top  $k$  eigenvectors (principal loadings) of the covariance matrix. Then the projected matrix  $Z \in \mathbb{R}^{n \times k}$  onto  $k$ -dimensional space is given by  $Z = X_C W$ , which represents the low dimensional embeddings.

KPCA extends PCA to handle nonlinear data structures by applying kernel functions to project the original data into a higher-dimensional feature space and then performing PCA in that space [21, 22]. Common kernel functions include Gaussian, polynomial, and sigmoid kernels. KPCA constructs the kernel matrix  $K$  for a dataset using a kernel function, where each entry is defined as  $K_{ij} = K(X_i, X_j) = \langle \phi(X_i), \phi(X_j) \rangle$  and  $\phi$  is a nonlinear mapping that transforms the original data from the input space into a possibly much higher-dimensional feature space, and centers the kernel matrix by  $\tilde{K} = HKH$ , where  $H = I_n - \frac{1}{n} \mathbf{1}\mathbf{1}^\top$  and  $\mathbf{1} \in \mathbb{R}^n$  is the vector of all ones [42]. After spectral decomposition on  $\tilde{K}$ , we have the projection of a new data point  $X$  onto the  $k$ th principal direction as the  $k$ th principal component:

$$Z_k(X) = \sum_{i=1}^n \alpha_{i,(k)} \tilde{K}(X_i, X), \quad (13)$$

where  $\alpha_{(k)} = (\alpha_{1,(k)}, \dots, \alpha_{n,(k)})^\top$  is the normalized eigenvector of the centered kernel matrix associated with the  $k$ -th eigenvalue. KPCA can capture nonlinear relationships in the data, whereas linear methods such as PCA are limited.

### 2.3 SIR and KSIR

SIR is designed for regression and classification tasks and focuses on projecting data onto a lower-dimensional subspace that captures most of the information about the response variable [23]. It begins by standardizing the features as  $U_i = \hat{\Sigma}^{-\frac{1}{2}}(X_i - \bar{X})$ , where  $\hat{\Sigma}_X$  is the sample covariance matrix of  $X$ , and slices the range of the response variable  $Y$  into  $H$  non-overlapping slices with  $n_h$  observations in the slice  $S_h$ ,  $h = 1, \dots, H$ . It then constructs the covariance of the slice means, weighted by their proportions:

$$\hat{V} = \sum_{h=1}^H p_h \hat{m}_h \hat{m}_h^\top,$$

where  $p_h$  is the proportion of observations in  $S_h$  and  $\hat{m}_h$  is the sample mean of the features in  $S_h$  [23]. SIR performs a spectral decomposition of  $\hat{V}$  and maps the eigenvector back to the original feature space to estimate the effective dimension reduction (EDR) directions. Specifically, if  $\hat{v}_k$  is the  $k$ th eigenvector of  $\hat{V}$ , the corresponding EDR direction is  $\hat{\beta}_k = \hat{\Sigma}_X^{-\frac{1}{2}} \hat{v}_k$ ,  $k = 1, \dots, d$ . We choose the first few leading EDR directions and project the data onto them to obtain  $\hat{Z}_i$ , the low-dimensional representation of  $X_i$ , as:

$$\hat{Z}_i = \hat{B}^\top (X_i - \bar{X}), \quad \hat{B} = (\hat{\beta}_1, \dots, \hat{\beta}_d). \quad (14)$$

The structural dimension  $d$  can be selected via information criteria, hypothesis tests, or cross-validation methods.

KSIR extends SIR by incorporating the kernel method similar to KPCA [43, 44, 45]. Let  $K_{ij} = K(X_i, X_j) = \langle \phi(X_i), \phi(X_j) \rangle$  map features into a high-dimensional reproducing kernel Hilbert space (RKHS), and let  $K \in \mathbb{R}^{n \times n}$  denote the kernel matrix with entries  $K_{ij}$  with a centered version  $\tilde{K} = HKH$ , where  $H = I_n - \frac{1}{n} \mathbf{1}\mathbf{1}^\top$ , similar to that of KPCA. The response variables  $Y_1, \dots, Y_n$  are divided into  $H$  slices. For each slice  $h$ , let  $\bar{K}_h$  denote the mean of the kernel features within that slice, defined as  $\bar{K}_h = \frac{1}{n_h} \sum_{i \in \mathcal{S}_h} \tilde{K}_{\cdot i}$ , where  $\mathcal{S}_h$  is the index set of samples in slice  $h$ ,  $n_h$  is the number of samples in that slice, and  $\tilde{K}_{\cdot i}$  represents the  $i$ -th column of the centered kernel matrix  $\tilde{K}$ . The overall mean of the kernel features is  $\bar{K} = \frac{1}{n} \sum_{i=1}^n \tilde{K}_{\cdot i}$ .

KSIR estimates the between-slice covariance matrix in the RKHS as

$$M = \sum_{h=1}^H p_h (\bar{K}_h - \bar{K})(\bar{K}_h - \bar{K})^\top,$$

where  $p_h = \frac{n_h}{n}$  is the proportion of samples in slice  $h$ . The nonlinear effective dimension reduction (EDR) directions are obtained by solving the generalized eigenvalue problem

$$\tilde{K} E_H \tilde{K} \alpha = \lambda \tilde{K} \tilde{K} \alpha.$$

where  $E_H = \sum_{h=1}^H \frac{\delta_h \delta_h^\top}{n_h}$ ,  $\delta_h = [\delta_h(y_1) \cdots \delta_h(y_n)]^\top$ , and  $\delta_h(y_i)$  is an indicator function representing if  $y_i$  is within slice  $h$ . Finally, the projection of a new observation  $X$  onto the  $k$ -th leading KSIR direction is given by

$$Z_k(X) = \sum_{i=1}^n \alpha_{i,(k)} K(X_i, X),$$

where  $\alpha_{(k)} = (\alpha_{1,(k)}, \dots, \alpha_{n,(k)})^\top$  is the  $k$ -th leading eigenvector. KSIR captures complex nonlinear relationships between the predictors and the response, which can provide improved performance in cases where traditional SIR fails to uncover nonlinear structures [46].

## 2.4 t-SNE

t-SNE is a nonlinear dimensionality reduction method that aims to preserve local structures in the data, commonly used for visualization in two or three dimensions. It minimizes the divergence between two probability distributions: one representing pairwise similarities in the high-dimensional space and the other in the low-dimensional space[35]. In the high-dimensional space, t-SNE applies a Gaussian distribution to model similarities between data points as

$$p_{j|i} = \frac{\exp\left(-\frac{\|X_i - X_j\|^2}{2\sigma_i^2}\right)}{\sum_{k \neq i} \exp\left(-\frac{\|X_i - X_k\|^2}{2\sigma_i^2}\right)}, \quad (15)$$

and symmetrizes the result with

$$p_{ij} = \frac{p_{j|i} + p_{i|j}}{2n}. \quad (16)$$

In the low-dimensional space, it utilizes a Student t-distribution with one degree of freedom to model similarities between points. Let  $Z_i \in \mathbb{R}^d$  and  $Z_j \in \mathbb{R}^d$  denote the low-dimensional embeddings corresponding to the high-dimensional data points  $X_i$  and  $X_j$ . The similarity between points  $i$  and  $j$  in the low-dimensional space is defined as

$$q_{ij} = \frac{(1 + \|Z_i - Z_j\|^2)^{-1}}{\sum_{k \neq l} (1 + \|Z_k - Z_l\|^2)^{-1}}, \quad (17)$$

which corresponds to a student’s t-distribution with one degree of freedom, and t-SNE minimizes the Kullback–Leibler divergence between the two distributions:

$$C = \sum_{i \neq j} p_{ij} \log \frac{p_{ij}}{q_{ij}} \quad (18)$$

over  $Z_i$ ,  $i = 1, \dots, n$ , to preserve the similarities of high-dimensional data points as much as possible in the low-dimensional space[36].

### 3 Numerical studies

In this section, we introduce the datasets used in this study and describe the evaluation process. We generate features from three types of distributions and simulate response variables using four different models for each type of feature distribution to create diverse datasets for evaluation. Among the four different models, three produce continuous response variables, while the fourth generates binary outcomes.

#### 3.1 Simulation settings

The feature samples  $X_i$  ( $i = 1, \dots, n$ ) are generated independently from each of the three distributions:

- (a) Independent Gaussian features:  $X_i \sim N(0, I_p)$ ,
- (b) Independent Non-Gaussian features:  $X_i \sim (1/2)N(-1_p, I_p) + (1/2)N(1_p, I_p)$ ,
- (c) Correlated Gaussian features:  $X_i \sim N(0, 0.6I_p + 0.41_p1_p^T)$ ,

where  $I_p$  denotes an identity matrix of dimension  $p$  and  $1_p$  denotes a  $p$ -dimensional vector with elements all equal to 1.

For the features generated from each of the above, we simulate four distinct types of response variables based on the following models:

**Continuous response variables:** • Model 1:  $Y_i = \sqrt[3]{\sum_{j=1}^s X_{ij}^3} + \log\left(\sqrt{\sum_{j=1}^s X_{ij}^2}\right) + \epsilon_j$ ,  
 • Model 2:  $Y_i = \sum_{j=1}^s \frac{X_{ij}}{1+e^{X_{ij+1}}} + \epsilon_j$ , • Model 3:  $Y = \sin\left(\frac{\pi \sum_{j=1}^s X_{ij}}{10}\right) + \epsilon_j$ , where  $X_{ij}$  is the  $j$ th element of  $X_i$ ,  $\epsilon_j$  is the random error, identically and independently distributed as  $N(0, 0.25)$  and independent of  $X_i$ , and  $s$  is the number of features related to the response variable.

**Categorical response variable:** • Model 4:  $P(Y_i = 1 | X_i) = \frac{1}{1+\exp(-(\beta_0+\sum_{j=1}^s \beta_j X_{ij}))}$ , where  $s$  is the number of features that are related to the probability of generating a binary response,  $\beta_0$  is set to .5,  $\beta_1, \dots, \beta_s$  are randomly generated from a uniform distribution  $\text{Unif}(-2, 2)$ , and the binary response variables  $Y_i$ ,  $i = 1, \dots, n$ , are generated from a Bernoulli distribution with event probabilities  $P(Y_i|X_i)$ .

Therefore, we have a total of 12 simulated data settings. This allows us to evaluate the performance of different dimensionality reduction methods under various data conditions and models. We generate each dataset with a sample size  $n = 1000$ , a feature dimension  $p = 500$ , and the number of features that are related to the response variable  $s = 10$ . We partition each dataset into training data and testing data using a 50-50 ratio, using training data to estimate dimensionality reduction and train predictive models, and then transforming the testing data into embeddings based on the trained models for future effectiveness evaluation. To account for the influence of random variation, we generate 100 datasets for each setting, perform training and testing splits, and estimate the dimensionality reduction using the procedure described above, and then compute the mean and standard error of the predicted results over the 100 datasets for both training and testing sets for final comparisons.

### 3.2 Real Data

We apply the public Fashion-MNIST dataset to compare the performance of different dimensionality reduction methods for image classification. The Fashion-MNIST dataset consists of images of fashion items and serves as a more complex alternative to the original MNIST

dataset of handwritten digits [47]. The higher complexity arises from the subtle differences between classes, making it a suitable benchmark for evaluating dimensionality reduction techniques in the context of image data [48]. The Fashion-MNIST dataset consists of 70,000 grayscale images [49, 50]. Each image has  $28 \times 28$  pixels, representing fashion items. There are 10 classes in the response variable corresponding to different types of clothing and accessories, such as T-shirts, trousers, pullovers, dresses, coats, sandals, shirts, sneakers, bags, and ankle boots. The entire dataset is partitioned into a training dataset with 60,000 images and a test set with 10,000 images [51]. By applying the dimensionality reduction methods to real-world image data, we evaluate their practical effectiveness and generalization beyond simulated datasets.

The other real data used in this study is the Online News Popularity dataset with a numerical response variable [52]. It contains 39,644 data points extracted from news articles published by Mashable over a two-year period. Each record corresponds to a single article and includes 60 explanatory variables, such as content-based statistics, sentiment and readability measures, keyword metrics, and dummy-coded indicators for publication day and topical category. The response is the number of social media shares an article receives. Because the distribution of the response variable is highly right-skewed, we apply a log transformation before modeling the data. To account for the influence of randomness, we repeat the train–test random sampling 100 times. For each split, we partition the training and testing sets with an equal size, use the training data to estimate dimensionality reduction (or embedding), and then employ it to embed the testing data for further evaluation.

### **3.3 Evaluation Procedure**

After dimensionality reduction, we employ the K-Nearest Neighbors (KNN) algorithm to evaluate the effectiveness of the reduced representations for subsequent predictions. KNN is a non-parametric learning algorithm that can be used for both classification and regression tasks [53, 54, 55].

In this study, KNN serves as a consistent evaluation method across different dimensionality reduction techniques. By applying KNN to the training and testing embeddings produced by each method, we assess how well the essential structure and information necessary for accurate predictions are preserved during dimensionality reduction. A higher prediction accuracy rate for classification problems or a lower mean squared error (MSE) for regression problems indicates that the dimensionality reduction method has effectively retained the relevant information from the original data [55].

## 4 Numerical results

### 4.1 Results for simulation data with continuous responses

To assess the performance of supervised UMAP on datasets with continuous responses, we utilize the response information in three distinct ways during model fitting.

- Method 1: Treat it as the original continuous variable, and apply the supervised UMAP with the edge weights defined by (12).
- Method 2: Treat it as a categorical variable with each unique response value representing a class, and apply the supervised UMAP with edge weights defined by (7).
- Method 3: Treat it as a categorical variable by slicing the response values into several intervals and treat each interval as a category to replace the original values, and then apply the supervised UMAP with edge weights defined by (7).

Here Method 1 and Method 2 are two approaches used in the existing supervised UMAP literature for data with continuous responses, whereas Method 3 is an approach that we design to reduce overfitting from Method 1. Note that Method 2 assigns equal weight to each response. As a result, the response information contributes very little to the dimensionality reduction step, and Method 2 behaves almost the same as unsupervised UMAP.

We evaluate the performance of the dimensionality reduction methods on the simulated datasets with continuous responses by comparing the MSE of KNN regression models trained on the embedded datasets, using the MSE of KNN regression models on the original datasets as the reference. The abbreviations used in the tables below are defined as follows:

- Orig: Original data without dimension reduction;
- SSU: Embeddings from supervised UMAP based on Method 3 (with sliced responses);
- CaSU: Embeddings from supervised UMAP based on Method 2;
- CoSU: Embeddings from supervised UMAP based on Method 1;
- UU: Unsupervised UMAP.

#### 4.1.1 Results for Model 1 with features generated from (a), (b), and (c)

The first performance comparison is conducted on datasets in which the response variables are generated according to Model 1 and the predictors are independently drawn from distributions (a), (b), and (c) described in Section 3.1. The training MSEs, testing MSEs, and the corresponding standard errors of the testing MSEs are summarized in Table 1. Across the three datasets a1, b1, and c1, SIR consistently achieves the lowest or near-lowest testing MSEs and testing standard errors, and yields more accurate predictions than models fitted to the original data without dimensionality reduction, indicating both stable performance and effective dimension reduction. Among the UMAP-based methods, CoSU generally exhibits the highest testing MSE, suggesting that the response information is not being effectively incorporated into the dimensionality reduction procedure. The supervised variant SSU mitigates some degree of overfitting observed in CoSU. However, it does not lead to performance improvements relative to the unsupervised UMAP method (UU). In addition, KSIR and t-SNE display substantial variability in testing performance for certain datasets, implying sensitivity to the underlying data structure and sampling variability.

Intuitively, supervised methods are expected to outperform unsupervised approaches because they explicitly leverage information from the response variable. However, the supervised UMAP approach CoSU yields among the highest testing MSEs and performs worse than its unsupervised counterpart, suggesting that response information is not effectively incorporated into the current supervised UMAP framework for dimension reduction. In contrast, the linear supervised method SIR consistently achieves relatively small MSEs. This shows that SIR is able to more effectively exploit response information and capture the underlying predictor–response relationships.

Table 1: Results for Model 1 based on datasets a1, b1, and c1

Model	Type	Orig	SSU	CaSU	CoSU	UU	PCA	KPCA	SIR	KSIR	t-SNE
a1	TrainMSE	3.3459	2.1683	3.7582	0.1994	3.7164	3.8525	3.8705	1.2472	0.1088	3.7320
	TestMSE	6.8812	8.5625	7.9132	9.8923	7.9246	7.7648	7.7688	5.6527	11.5459	7.9251
	TestSE	0.0426	0.0597	0.0492	0.1286	0.0558	0.0482	0.0485	0.0391	0.0610	0.0382
b1	TrainMSE	1.8150	0.9296	2.0119	0.1731	2.0029	2.0205	2.0525	0.9621	0.3177	1.9781
	TestMSE	3.7325	4.7323	4.1784	10.0831	4.1348	4.0642	4.1327	3.1404	54.1738	46.5391
	TestSE	0.0261	0.0422	0.0328	0.6822	0.0313	0.0307	0.0326	0.0288	0.2597	4.3907
c1	TrainMSE	1.2051	0.8454	1.3014	0.1356	1.3078	1.2686	1.2840	1.1590	0.3106	1.2499
	TestMSE	2.4139	2.9321	2.7095	4.3873	2.6795	2.5472	2.5896	2.5951	17.5376	10.1491
	TestSE	0.0170	0.0214	0.0205	0.1822	0.0188	0.0189	0.0215	0.0193	0.1302	0.9223

#### 4.1.2 Results for Model 2 with features generated from (a), (b), and (c)

The evaluation in this section is conducted on datasets where the response variables are generated according to Model 2, and the predictors are generated independently from distributions (a), (b), and (c). The datasets are represented as a2, b2, and c2 in Table 2. The corresponding training and testing MSEs, along with the standard errors of the testing MSEs, are summarized in Table 2. Consistent with the findings of Model 1, SIR again achieves the lowest MSE test in all settings, demonstrating robust and advantageous performance among the dimensionality reduction methods considered. PCA and UU exhibit comparable performance, maintaining relatively moderate testing MSEs and indicating reasonable stability across the different data-generating distributions. In contrast, the supervised UMAP approach CoSU continues to display clear signs of overfitting, resulting in inferior performance.

More broadly, the comparison between the three supervised UMAP variants and the unsupervised methods consistently suggests that the incorporation of response information within the current supervised UMAP framework does not translate into improved predictive performance. This pattern is also seen from the results of Model 1. This highlights a potential limitation of existing supervised UMAP approaches and motivates further investigation into more effective strategies for integrating response information into nonlinear manifold learning methods in the regression setting.

Table 2: Results for Model 2 based on datasets a2, b2, and c2

Model	Type	Orig	SSU	CaSU	CoSU	UU	PCA	KPCA	SIR	KSIR	t-SNE
a2	TrainMSE	1.8710	1.1763	2.0956	0.1249	2.0753	2.1044	2.1242	0.5773	0.1098	2.0647
	TestMSE	3.6844	4.6437	4.2859	5.2758	4.2849	4.2955	4.2922	2.5370	6.3686	4.3799
	TestSE	0.0281	0.0334	0.0386	0.0900	0.0321	0.0307	0.0374	0.0208	0.0404	0.0323
b2	TrainMSE	2.5760	1.2935	2.9138	0.2829	2.8395	2.8876	2.9560	1.0956	0.3750	2.8810
	TestMSE	5.0703	6.7569	5.8695	13.6292	5.9508	5.7387	5.9544	3.9864	58.3359	55.5305
	TestSE	0.0521	0.0760	0.0634	0.8127	0.0634	0.0571	0.0568	0.0469	0.2939	4.6483
c3	TrainMSE	0.3142	0.1971	0.3283	0.0541	0.3282	0.3191	0.3223	0.3040	0.0131	0.3173
	TestMSE	0.6308	0.7446	0.6650	0.8559	0.6667	0.6415	0.6497	0.6596	1.5164	0.9659
	TestSE	0.0040	0.0055	0.0040	0.0171	0.0039	0.0038	0.0039	0.0040	0.0083	0.0346

#### 4.1.3 Results for Model 3 with features generated from (a), (b), and (c)

The response variables in these datasets are generated according to Model 3, and the predictors are generated independently from distributions (a), (b), and (c). The datasets are named as a3, b3, and c3 in Table 3. Under Model 3, the results exhibit patterns that are largely consistent with those observed for the previous models. SIR once again achieves the lowest testing MSE across all considered datasets and demonstrates stable and robust performance across different data-generating mechanisms. PCA and UU also attain comparably low testing errors, indicating that they provide relatively effective dimensionality reduction in this setting. In contrast, the supervised UMAP approach CoSU continues to yield slightly higher testing MSEs across all datasets, suggesting that the incorporation of response information in its current form does not lead to improved predictive performance.

Table 3: Results for Model 3 based on datasets a3, b3, and c3

Model	Type	Orig	SSU	CaSU	CoSU	UU	PCA	KPCA	SIR	KSIR	t-SNE
a3	TrainMSE	0.4262	0.2548	0.4568	0.0421	0.4537	0.4583	0.4584	0.1629	0.0134	0.4548
	TestMSE	0.8458	1.0307	0.9301	1.2168	0.9243	0.9283	0.9315	0.6927	1.3777	0.9384
	TestSE	0.0047	0.0074	0.0069	0.0203	0.0069	0.0060	0.0075	0.0039	0.0071	0.0052
b3	TrainMSE	0.4345	0.2645	0.4593	0.0532	0.4529	0.4687	0.4668	0.1946	0.0139	0.4541
	TestMSE	0.8587	1.0295	0.9298	1.2990	0.9236	0.9167	0.9230	0.7074	1.3890	0.9463
	TestSE	0.0049	0.0064	0.0068	0.0244	0.0058	0.0049	0.0060	0.0050	0.0078	0.0150
c3	TrainMSE	0.3142	0.1971	0.3283	0.0541	0.3282	0.3191	0.3223	0.3040	0.0131	0.3173
	TestMSE	0.6308	0.7446	0.6650	0.8559	0.6667	0.6415	0.6497	0.6596	1.5164	0.9659
	TestSE	0.0040	0.0055	0.0040	0.0171	0.0039	0.0038	0.0039	0.0040	0.0083	0.0346

## 4.2 Results for simulation data with categorical responses

The evaluation in this section is conducted on datasets with categorical responses, where the response variables are generated according to Model 4 and the predictors are drawn from distributions (a), (b), and (c). The datasets are named as a4, b4, and c4 in Table 4. To assess classification performance, we compare misclassification error rates obtained from KNN classification applied to the embedded test datasets as well as to the original test data. The corresponding training error rates (TrainError), testing error rates (TestError), and the standard errors of the testing error rates, computed from 100 random repetitions, are reported in Table 4.

Because the response variable is categorical, the CaSU and SSU approaches coincide and therefore produce identical results, while CoSU is not applicable in this setting. Accordingly, CoSU and SSU are not reported in Table 4.

As shown in Table 4, the supervised UMAP method CaSU and SIR outperform the other dimensionality reduction approaches on the test datasets. In this classification setting, supervised UMAP exhibits strong performance and achieves competitive classification accuracy. These results suggest that, in contrast to the regression settings, response information is more effectively incorporated in the supervised UMAP framework when the response is categorical. Correspondingly, supervised UMAP provides clear improvements over its unsupervised method in terms of predictive performance. These findings indicate that, when appropriately

Table 4: Results (misclassification rate) for Model 4 based on datasets a4, b4, and c4

Model	Type	Orig	CaSU	UU	PCA	KPCA	SIR	KSIR	t-SNE
Data_a4	TrainError	0.223	0.033	0.243	0.246	0.246	0.087	0.013	0.242
	TestError	0.451	0.447	0.490	0.493	0.495	0.357	0.496	0.495
	TestSE	0.002	0.002	0.002	0.003	0.003	0.003	0.002	0.002
Data_b4	TrainError	0.156	0.039	0.167	0.170	0.172	0.141	0.011	0.164
	TestError	0.286	0.280	0.304	0.304	0.307	0.284	0.495	0.510
	TestSE	0.015	0.014	0.015	0.015	0.016	0.013	0.002	0.023
Data_c4	TrainError	0.197	0.039	0.206	0.205	0.207	0.173	0.012	0.199
	TestError	0.370	0.358	0.387	0.392	0.392	0.370	0.493	0.461
	TestSE	0.008	0.008	0.008	0.009	0.008	0.007	0.002	0.010

leveraged, response information in the supervised UMAP framework can enhance prediction accuracy for supervised learning tasks.

### 4.3 Results for real data with categorical responses

The first real data used in our application is the Fashion-MNIST dataset described in Section 3.2. Table 5 reports the misclassification error rate for each method on both the training and testing datasets, along with the elapsed time (in seconds) for model fitting, data transformation, and evaluation.

Table 5: Results (misclassification rate) for Fashion-MNIST dataset

Type	TrainError	TestError	Elapsed Time (sec)
Original	0.080	0.146	40.524
UMAP Supervised	0.018	0.162	18.909
UMAP Unsupervised	0.145	0.247	13.922
PCA	0.305	0.517	1.301
KPCA	0.305	0.515	35.173
SIR	0.292	0.498	1.125
KSIR	0.470	0.762	8.474
t-SNE	0.092	0.504	220.947

The original data achieves balance between training and testing performance without dimensionality reduction and serves as the baseline for comparison. Supervised UMAP

delivers the strongest training results, and its testing misclassification rate remains close to that of the original data after compressing the 784-dimensional features into two-dimensional embeddings. Figure 1 displays the reduced two-dimensional embeddings for both the training and testing sets, colored by fashion-item class. The visualization shows that supervised UMAP cleanly separates the training data into the expected classes while preserving the global structure. The testing data aligns well with this structure, exhibiting clear class separation and producing the highest prediction accuracy. For consistency across comparisons and for ease of visualization, we set the embedding dimension to 2. Results obtained with higher dimensional embeddings, or with embeddings obtained by cross-validation show a similar pattern.

In contrast, unsupervised UMAP shows reduced performance on both the training and testing sets, and the corresponding scatter plots reveal a noticeable decline in embedding quality. For both training and testing datasets, class boundaries are less distinct than those in the supervised embeddings, and some regions, particularly in the lower-right portion of the plot, show substantial mixing of classes.

PCA and SIR are fast but less effective for this large-scale dataset. They show higher misclassification error rates than the UMAP methods. Both PCA and SIR are linear embedding methods, focusing on maximizing variance or preserving sufficient effective reductions using linear transformations. However, the Fashion-MNIST dataset has complex, non-linear embedding patterns that PCA and SIR might not be able to capture. Neither KPCA nor KSIR performs better than their non-kernel counterparts on this dataset. Similar to the misclassification rates, their embedding plots show less clear boundaries and less effective embeddings for classification.

t-SNE takes the longest time to run while achieving a strong training score; However, its test score is relatively weak, likely due to a lack of a global transformation that can be adapted to the test dataset.

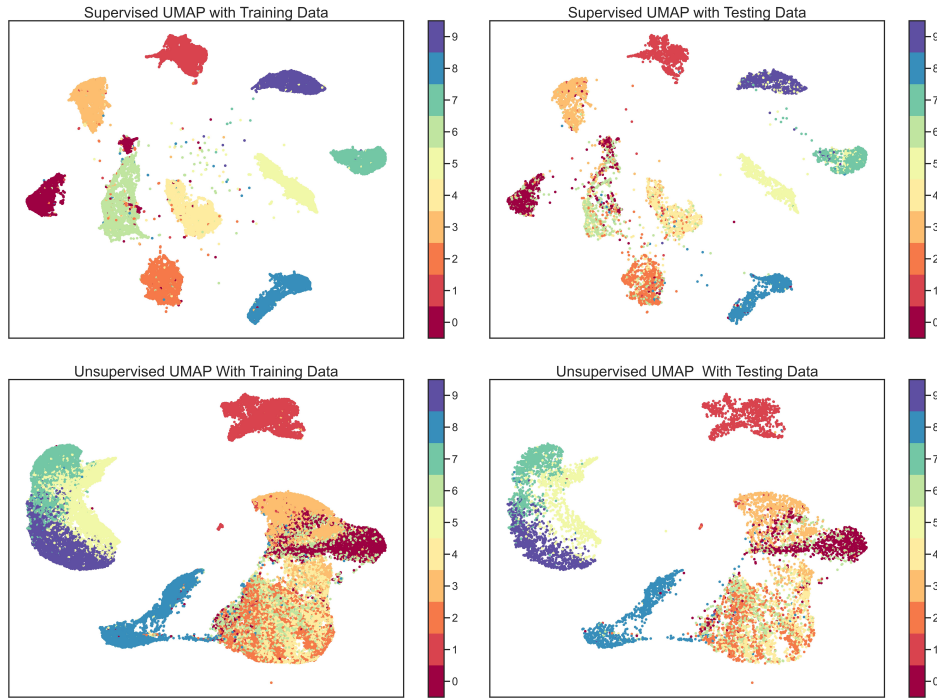


Figure 1: Performance plots of UMAP

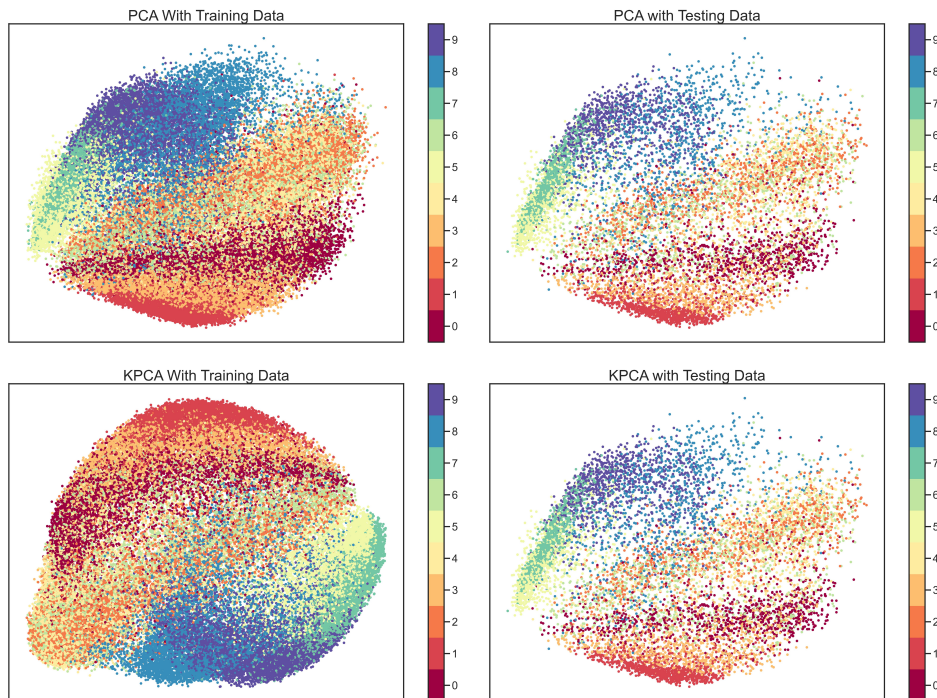


Figure 2: Performance plots of PCA and KPCA

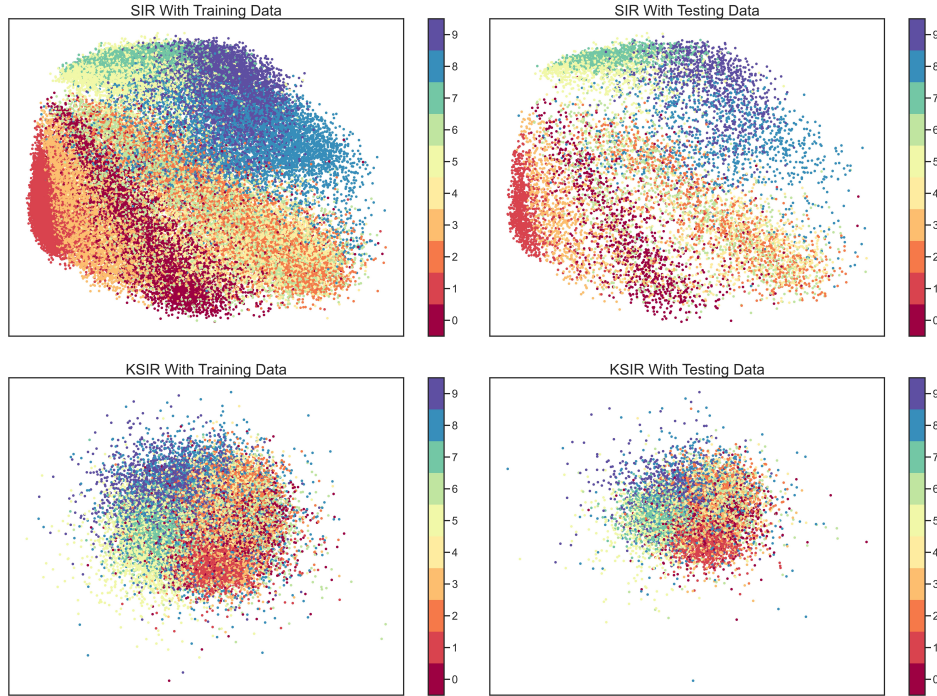


Figure 3: Performance plots of SIR and KSIR

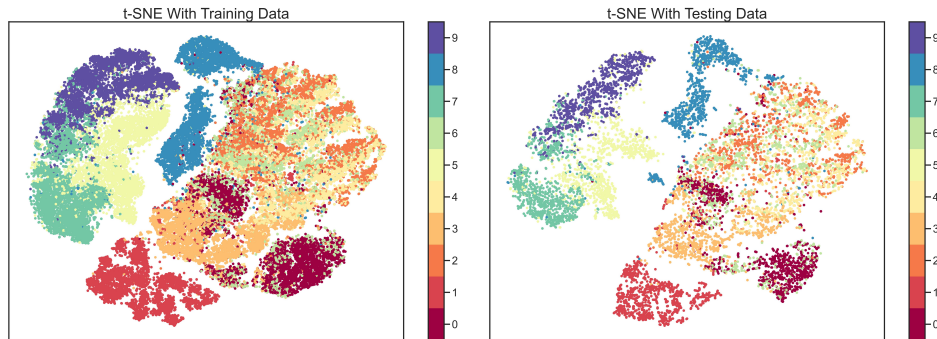


Figure 4: Performance plot of t-SNE

#### 4.4 Results for real data with continuous responses

The second real data studied in our application is the Online News Popularity dataset described in Section 3.2. Table 6 presents the performance comparison on the Online News Popularity dataset. The numerical results are largely consistent with the patterns observed in our simulation studies. Among all the dimension reduction methods, SIR and KSIR achieve the lowest testing MSEs and SEs, and therefore perform the best overall. KSIR,

in particular, attains the lowest testing MSE on this dataset. SSU, CaSU, and UU offer moderate improvements over PCA, while CoSU again produces a higher testing MSE than UU and SSU on this numerical response dataset.

The results again indicate the limitations of existing supervised UMAP approaches, which do not fully leverage response information for prediction tasks in regression settings, and motivate further investigation on more effective strategies for integrating response information into nonlinear manifold learning methods for regression.

Table 6: Results for the Online News Popularity dataset

Type	Orig	SSU	CaSU	CoSU	UU	PCA	KPCA	SIR	KSIR	t-SNE
TrainMSE	0.5097	0.4874	0.5299	0.3860	0.5291	0.5537	0.5771	0.5009	0.4544	0.5212
TestMSE	1.0231	1.0946	1.0694	1.2964	1.0702	1.1071	1.1938	1.0049	0.9774	1.1914
TestSE	0.0009	0.0010	0.0011	0.0013	0.0011	0.0010	0.0397	0.0010	0.0009	0.0027

## 5 Conclusion

This study investigates UMAP and other dimension reduction methods, including PCA, SIR, Kernel PCA, Kernel SIR, and t-SNE, in both supervised and unsupervised frameworks for regression and classification tasks and evaluates their performances using simulated and real-world datasets. KNN was applied to evaluate the prediction performance for both training and testing datasets, with the number of neighbors tuned and random seeds to ensure reproducible results across runs. UMAP exhibited strong performance for classification tasks on simulated datasets and real examples by effectively preserving both local and global data structures, making it a highly effective method for complex datasets with categorical responses. In the simulated settings with continuous responses, supervised linear dimension reduction method SIR achieved better results than the UMAP methods. The supervised UMAP method CoSU yielded nearly the highest testing MSEs and performed less effectively than the unsupervised UMAP and other dimension methods, suggesting that the current supervised UMAP method did not fully utilize the information from continuous responses

during the embedding process. Future work on improving supervised UMAP under the continuous response setting is worthy of further investigation.

Overall, UMAP remains a powerful and versatile tool for dimensionality reduction and offers a strong balance of accuracy and computational efficiency in classification contexts. Its supervised extensions, however, demonstrate limitations in incorporating numerical response information effectively, which points to an important direction for future research on improving supervised UMAP in regression settings.

## References

- [1] Christopher J. C. Burges. Dimension reduction: A guided tour. *Foundations and Trends in Machine Learning*, 2(4):275–365, 2010.
- [2] Geoffrey E. Hinton and Ruslan R. Salakhutdinov. Reducing the dimensionality of data with neural networks. *Science*, 313(5786):504–507, 2006.
- [3] Ian Goodfellow, Yoshua Bengio, Aaron Courville, and Yoshua Bengio. *Deep learning*, volume 1. MIT press Cambridge, 2016.
- [4] Etienne Becht, Leland McInnes, John Healy, Charles-Antoine Dutertre, Immanuel W. H. Kwok, Lai Guan Ng, Florent Ginhoux, and Evan W. Newell. Dimensionality reduction for visualizing single-cell data using umap. *Nature Biotechnology*, 37(1):38–44, 2019.
- [5] Richard E. Bellman. *Adaptive Control Processes: A Guided Tour*. Princeton University Press, 1961.
- [6] Christopher M Bishop and Nasser M Nasrabadi. *Pattern recognition and machine learning*, volume 4. Springer, 2006.
- [7] Trevor Hastie, Robert Tibshirani, Jerome Friedman, et al. *The elements of statistical learning*, 2009.

- [8] Laurens Van Der Maaten, Eric O Postma, H Jaap Van Den Herik, et al. Dimensionality reduction: A comparative review. *Journal of machine learning research*, 10(66-71):13, 2009.
- [9] Leland McInnes, John Healy, and James Melville. Umap: Uniform manifold approximation and projection for dimension reduction. *arXiv preprint arXiv:1802.03426*, 2018.
- [10] Tim Sainburg, Leland McInnes, and Timothy Q. Gentner. Parametric umap: Learning embeddings with deep neural networks for representation and visualization. *arXiv preprint arXiv:2009.12981*, 2021.
- [11] Marius Pachitariu, Carsen Stringer, and Kenneth D. Harris. Robustness of spike sorting to neural noise using umap. *Nature Neuroscience*, 22(12):1925–1935, 2019.
- [12] Bartosz Szubert, John E. Cole, Claudia Monaco, and Ignat Drozdov. Structure-preserving visualisation of high dimensional single-cell datasets using umap. *Scientific Reports*, 9(1):1–10, 2019.
- [13] Alex Diaz-Papkovich, Luke Anderson-Trocmé, Chief Ben-Eghan, and Simon Gravel. Umap reveals cryptic population structure and phenotype heterogeneity in large genomic cohorts. *PLoS genetics*, 15(11):e1008432, 2019.
- [14] Dmitry Kobak and Philipp Berens. The art of using t-sne for single-cell transcriptomics. *arXiv preprint arXiv:1902.02115*, 2019.
- [15] Mourad Allaoui, Mohammed Lamine Kherfi, and Mohamed Cheriet. Deep embeddings for high-dimensional data visualization using umap. *Pattern Recognition Letters*, 137:48–55, 2020.
- [16] Karl Pearson. On lines and planes of closest fit to systems of points in space. *Philosophical Magazine*, 2(11):559–572, 1901.

- [17] Harold Hotelling. Analysis of a complex of statistical variables into principal components. *Journal of Educational Psychology*, 24(6):417–441, 1933.
- [18] Ian T. Jolliffe. *Principal Component Analysis*. Springer, 2nd edition, 2002.
- [19] Richard Cangelosi and Alain Goriely. Component retention in principal component analysis with application to cdna microarray data. *Biology Direct*, 2(1):2, 2007.
- [20] Jonathon Shlens. A tutorial on principal component analysis. *arXiv preprint arXiv:1404.1100*, 2014.
- [21] Bernhard Schölkopf, Alexander Smola, and Klaus-Robert Müller. Nonlinear component analysis as a kernel eigenvalue problem. *Neural Computation*, 10(5):1299–1319, 1998.
- [22] Sebastian Mika, Bernhard Schölkopf, Alexander Smola, Klaus-Robert Müller, Matthias Scholz, and Gunnar Rätsch. Kernel pca and de-noising in feature spaces. In *Advances in Neural Information Processing Systems*, volume 11, pages 536–542, 1999.
- [23] Ker-Chau Li. Sliced inverse regression for dimension reduction. *Journal of the American Statistical Association*, 86(414):316–327, 1991.
- [24] R. Dennis Cook. *Regression Graphics: Ideas for Studying Regressions*. Wiley, 2009.
- [25] R Dennis Cook. *Regression graphics: Ideas for studying regressions through graphics*. John Wiley & Sons, 2009.
- [26] Bing Li. *Sufficient dimension reduction: Methods and applications with R*. Chapman and Hall/CRC, 2018.
- [27] Peter Hall and Ker-Chau Li. On almost linearity of low dimensional projections from high dimensional data. *The Annals of Statistics*, 21(2):867–889, 1993.
- [28] Lexin Li and Xiangrong Yin. Sliced inverse regression with regularizations. *Biometrics*, 64(1):124–131, 2008.

- [29] Wei Qian, Shanshan Ding, and R Dennis Cook. Sparse minimum discrepancy approach to sufficient dimension reduction with simultaneous variable selection in ultrahigh dimension. *Journal of the American Statistical Association*, 2019.
- [30] Louis Ferré. Determining the dimension in sliced inverse regression. *Journal of the American Statistical Association*, 93(441):132–140, 1998.
- [31] Yingcun Xia, Howell Tong, W. K. Li, and Li-Xing Zhu. Adaptive regression by mixing. *Journal of the American Statistical Association*, 97(458):576–588, 2002.
- [32] Bing Li, Min Kyung Kim, and Naomi Altman. On dimension folding of matrix-or array-valued statistical objects. *The Annals of Statistics*, 38:1094–1121, 2010.
- [33] Shanshan Ding and R Dennis Cook. Tensor sliced inverse regression. *Journal of Multivariate Analysis*, 133:216–231, 2015.
- [34] Shanshan Ding, Wei Qian, and Lan Wang. Double-slicing assisted sufficient dimension reduction for high-dimensional censored data. 2020.
- [35] Laurens van der Maaten and Geoffrey Hinton. Visualizing data using t-sne. *Journal of Machine Learning Research*, 9(Nov):2579–2605, 2008.
- [36] Laurens van der Maaten. Accelerating t-sne using tree-based algorithms. *Journal of Machine Learning Research*, 15(1):3221–3245, 2014.
- [37] Martin Wattenberg, Fernanda Viégas, and Ian Johnson. How to use t-sne effectively. *Distill*, 2016.
- [38] Laurens Van Der Maaten. Accelerating t-sne using tree-based algorithms. *The journal of machine learning research*, 15(1):3221–3245, 2014.
- [39] George C. Linderman and Stefan Steinerberger. Clustering with t-sne, provably. *SIAM Journal on Mathematics of Data Science*, 1(2):313–332, 2019.

- [40] Leland McInnes, John Healy, and contributors. Umap api guide, 2025. Available at: <https://umap-learn.readthedocs.io/en/latest/api.html>.
- [41] Leland McInnes, John Healy, and contributors. Umap module source, 2025. Available at: [https://umap-learn.readthedocs.io/en/latest/\\_modules/umap/umap\\_.html](https://umap-learn.readthedocs.io/en/latest/_modules/umap/umap_.html).
- [42] Xiang Ma and Nicholas Zabaras. Kernel principal component analysis for stochastic input model reduction. *Journal of Computational Physics*, 230(19):7311–7331, 2011.
- [43] Bernhard Schölkopf and Alexander J. Smola. *Learning with Kernels: Support Vector Machines, Regularization, Optimization, and Beyond*. MIT Press, Cambridge, MA, 2002.
- [44] Han-Ming Wu. Kernel sliced inverse regression with applications to classification. *Journal of Computational and Graphical Statistics*, 17(3):590–610, 2008.
- [45] Yi-Ren Yeh, Su-Yun Huang, and Yuh-Jye Lee. Nonlinear dimension reduction with kernel sliced inverse regression. *IEEE Transactions on Knowledge and Data Engineering*, 21(11):1590–1603, 2009.
- [46] Qiang Wu, Feng Liang, and Sayan Mukherjee. Kernel sliced inverse regression: regularization and consistency. *Abstract and Applied Analysis*, 2013:Article ID 540725, 11 pages, 2013.
- [47] Han Xiao, Kashif Rasul, and Roland Vollgraf. Fashion-MNIST: A Novel Image Dataset for Benchmarking Machine Learning Algorithms. arXiv preprint, 2017. arXiv:1708.07747.
- [48] Ravil I. Mukhamediev. State-of-the-Art Results with the Fashion-MNIST Dataset. *Mathematics*, 12(20):3174, 2024.
- [49] TensorFlow Datasets. Fashion MNIST TensorFlow Datasets Documentation. Online documentation, 2024.
- [50] Keras. Fashion MNIST dataset Keras API Documentation. Online documentation, 2025.

- [51] GitHub. Fashion MNIST GitHub Repository. GitHub repository, 2017.
- [52] D. Dua and C. Graff. Online news popularity. <https://archive.ics.uci.edu/ml/datasets/Online+News+Popularity>, 2019. UCI Machine Learning Repository.
- [53] Thomas M. Cover and Peter E. Hart. Nearest neighbor pattern classification. *IEEE Transactions on Information Theory*, 13(1):21–27, 1967.
- [54] Naomi S. Altman. An introduction to kernel and nearest-neighbor nonparametric regression. *The American Statistician*, 46(3):175–185, 1992.
- [55] Trevor Hastie, Robert Tibshirani, and Jerome Friedman. *The Elements of Statistical Learning: Data Mining, Inference, and Prediction*. Springer, New York, 2nd edition, 2009.